JOURNAL OF Materials CHEMISTRY

Surface characterization of vinyl polymer–silica colloidal nanocomposites using X-ray photoelectron spectroscopy

M. J. Percy,[a] J. I. Amalvy,[a]† C. Barthet,[a] S. P. Armes,*[a] S. J. Greaves,[b] J. F. Watts[b] and H. Wiese[c]

[a]*School of Chemistry, Physics and Environmental Science, University of Sussex, Falmer, Brighton, UK BN1 9QJ. E-mail: s.p.armes@sussex.ac.uk*
[b]*School of Mechanical Engineering and Materials Science, University of Surrey, Guildford, Surrey, UK GU2 5XH*
[c]*BASF AG, ZKD/N-B 1 67056, Ludwigshafen, Germany*

Received 4th November 2001, Accepted 12th December 2001
First published as an Advance Article on the web 29th January 2002

We report the use of X-ray photoelectron spectroscopy (XPS) to characterize the surface compositions of colloidal nanocomposite particles. Each nanocomposite was synthesized by (co)polymerizing 4-vinylpyridine in the presence of an ultrafine silica sol. Thus, nitrogen and silicon were utilized as unique elemental markers for the (co)polymer and silica components, respectively, and the silicon/nitrogen atomic ratios determined by XPS were used to assess the surface compositions of the particles. For all the homopoly(4-vinylpyridine)–silica nanocomposites examined, the XPS surface compositions are comparable to the bulk compositions determined by thermogravimetric analyses and elemental microanalyses. This is consistent with the 'currant bun' particle morphologies observed by transmission electron microscopy (TEM) and indicates that the silica particles are uniformly distributed throughout the nanocomposite particles. In contrast, the particle surface of a poly(styrene-co-4-vinylpyridine)–silica nanocomposite is distinctly silica-rich, as judged by XPS; this suggests a core–shell morphology, with the silica component forming the shell and the hydrophobic copolymer forming the core. Both the 'currant bun' and core–shell particle morphologies are supported by TEM studies of nanocomposite particles sectioned using cryo-ultramicrotomy. A poly(methyl methacrylate-co-4-vinylpyridine)–silica nanocomposite shows an XPS surface composition which is intermediate between those found for the 'currant bun' particles and the core–shell particles. In view of its relatively high silica content, a 'raspberry' particle morphology, similar to that previously reported for conducting polymer–silica nanocomposites, is suggested. Finally, it is shown that, in the case of the poly(methyl methacrylate-co-4-vinylpyridine)–silica nanocomposite, it is possible to use the carbonyl carbon signal of the methyl methacrylate residues as an unambiguous marker for the copolymer component; the surface composition obtained from this alternative analysis is consistent with that calculated using the nitrogen XPS signal. This approach may be particularly useful for assessing the surface compositions of nanocomposites containing a relatively low (or zero) proportion of 4-vinylpyridine co-monomer.

Introduction

There is increasing interest in polymer-based nanocomposites. Since the pioneering work[1–3] by the Toyota group on nylon–clay nanocomposites, many benefits have been claimed for these materials, including improved mechanical properties and fire retardancy.[4] Applications in emerging technologies such as nonlinear optics,[5] microelectronics[6] and polymer LEDs[7] have also been reported. In many cases, pre-formed polymer chains are simply intercalated within the galleries or pores of layered compounds or zeolites.[8] In other studies, the polymeric component is generated by *in situ* polymerization. For example, Mark *et al.*[9] prepared monolithic poly(methyl acrylate)–SiO_2 nanocomposites by dispersing surface-modified silica particles in methyl acrylate, followed by polymerization of the monomeric continuous phase. The incorporation of silica particles into a polymer matrix resulted in great improvement in the thermal and flammability properties over the native polymer, without the detrimental effects normally associated with conventional fire retardants.[10,11]

In the context of *colloidal* nanocomposites, several groups have reported the synthesis of various new organic–inorganic hybrid particles. In general, these nanocomposites are prepared by carrying out an aqueous phase polymerization in the presence of an inorganic sol, typically silica. McQueston and Iler reported the synthesis of either urea or melamine formaldehyde–silica particles using step polymerization chemistry. On calcination to volatilize the copolymer component, highly porous, micrometer-sized silica particles were obtained, which were claimed to be a useful stationary phase for liquid chromatography.[12] More recently, Bourgeat-Lami and Lang described the synthesis of polystyrene–silica nanocomposite particles of 400 to 950 nm in diameter by dispersion polymerization in ethanol–water mixtures.[13] In this approach, silica sols of 50–120 nm diameter particles were pre-treated with a functional unsaturated siloxane to ensure reactive grafting of the growing polystyrene chains to the surface of the silica particles. In addition, a soluble polymeric stabilizer, poly(*N*-vinyl pyrrolidone), was utilized to maintain the colloidal stability of the dispersion. In later work, larger silica particles (up to 630 nm diameter) were utilized and core–shell morphologies were obtained, with complete encapsulation of the silica particles by the polystyrene occurring under certain conditions.[14]

In the 1990's, we reported the synthesis of a range of

†Member of CICPBA (Argentina). Permanent address: CIDEPINT, Av. 52 (e/121 y 122), (1900) La Plata, Argentina.

colloidal conducting polymer–silica particles by the oxidative polymerization of either aniline or pyrrole *via* dispersion polymerization in aqueous media.[15–20] Surface functionalization protocols were examined[21–23] and selected particles were evaluated as highly colored marker particles for immunodiagnostic assays.[24] More recently, we have extended these surfactant-free nanocomposite syntheses to include vinyl monomers using free radical polymerization chemistry.[25–27] Here it is usually necessary to use 4-vinylpyridine (4VP) as an auxiliary co-monomer in order to promote a strong interaction between the silica sols and the precipitating polymer phase (see Fig. 1). However, up to 90 mol% of the 4VP can be replaced by commodity comonomers such as styrene, methyl methacrylate or *n*-butyl (meth)acrylate. Thus, the copolymer Tg can be adjusted so that the nanocomposite particles are either non-film-forming or film-forming in nature. Due to the high degree of dispersion and small size of the silica sol, the film-forming nanocomposite formulations have some potential as tough, optically transparent, scratch-resistant coatings.[27]

Herein, we report a detailed X-ray photoelectron spectroscopy (XPS) study of the surface compositions of selected vinyl polymer–silica nanocomposites. XPS is a surface analytical technique with a typical sampling depth of 2–5 nm[28] and it is well suited to the interrogation of the surface compositions of colloidal particles.[29–33] In each case, non-film-forming formulations were chosen in order to assist the interpretation of the XPS data. The XPS data are combined with transmission electron microscopy studies of the ultramicrotomed particles in order to shed further light on the particle morphology. More specifically, we wished to distinguish between the most likely particle morphologies for these nanocomposites, see Fig. 2. In this paper, these four morphologies are termed 'currant bun', 'raspberry' and 'core–shell' (either polymer-based 'cores' or silica-based 'cores'), respectively.

Experimental

Nanocomposite synthesis. The vinyl polymer–silica nanocomposites were prepared by free radical polymerization of 4-vinylpyridine (4VP) in the presence of a 20 nm silica sol (Nyacol 2040; supplied as a 40 w/w% aqueous dispersion by Eka Chemicals, Bohus, Sweden; these particles possess a negative surface charge with sodium counter-ions). Thus, in a typical experiment, Nyacol 2040 (13.0 g, equivalent to 8.0 g of dry weight silica), de-ionized water (73 mL) and monomer(s) (5.0 mL) were added to a three-necked round-bottom flask, followed by degassing with nitrogen and heating to 60 °C. Ammonium persulfate initiator (50.0 mg, 1.0 wt.% based on monomer) dissolved in water (3.0 mL) was degassed and added to the reaction vessel. The reaction mixture was stirred at 60 °C for 24 h. The milky-white dispersions were purified by four centrifugation–re-dispersion cycles, with each successive supernatant being decanted and replaced with aqueous NaOH (pH

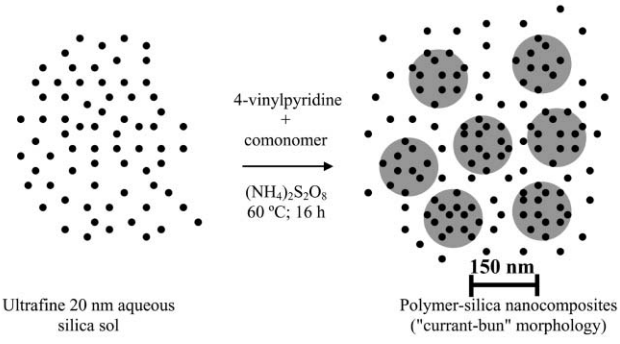

Fig. 1 Schematic representation of the formation of vinyl polymer–silica nanocomposite particles by the free-radical polymerization of 4VP at 60 °C in the presence of an ultrafine silica sol.

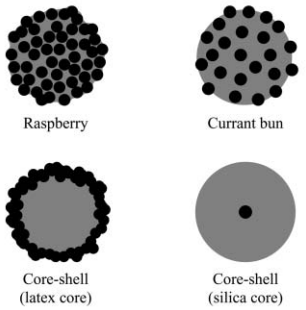

Fig. 2 Schematic representation of the possible nanocomposite particle morphologies.

10). Care was taken to avoid excessive centrifugation rates (no more than 5,000 rpm) and times (1–3 h), since these would otherwise result in the unwanted sedimentation of the excess silica sol and also make re-dispersion of the nanocomposite particles more difficult.

Nanocomposite characterization

Transmission electron microscopy. Dilute nanocomposite dispersions were dried onto carbon-coated copper grids and examined using either a Hitachi 7100 or a Zeiss 902 instrument operating at 75 and 80 kV, respectively. Cryo-ultramicrotomy studies were performed at −100 to −120 °C and the samples stained with RuO_4. The thickness of the cryo-sections was approximately 100 nm. Samples were examined using a Hitachi 7100 microscope operating at 100 kV.

Chemical composition. Thermogravimetric analyses were performed with a Perkin-Elmer TGA-7 instrument. Nanocomposite dispersions were dried at 50 °C overnight to yield dried powders. These powders were heated in air to 800 °C at a scan rate of 20 °C min^{-1} and the observed mass loss was attributed to the quantitative pyrolysis of the (co)polymer component. The silica content indicated by the incombustible residues was corrected for loss of surface moisture. CHN microanalyses were carried out at an external analytical laboratory (Medac Ltd., Egham, Surrey, UK).

Aqueous electrophoresis

Aqueous electrophoresis data were obtained using a Malvern Instruments Zetamaster instrument. The zeta potential, ζ, was calculated[34] from the electrophoretic mobility (u) using the Smoluchowsky relationship, $\zeta = \eta u/\varepsilon$, where it is assumed that $\kappa a \gg 1$ (where η is the solution viscosity, ε is the dielectric constant of the medium, and κ and a are the Debye–Hückel parameter and the particle radius, respectively). The solution pH was adjusted by the addition of NaOH or HCl.

X-Ray photoelectron spectroscopy

Measurements on poly(4-vinylpyridine)–silica nanocomposites were made using a VG Scientific ESCALAB Mk. II spectrometer interfaced to a VGS 5000S data system based on a DEC PDP 11/73 computer. An Mg-Kα X-ray source was operated at a power of 200 W (20 mA and 10 kV). The spectrometer was operated in the fixed analyzer transmission mode at a pass energy of 100 eV for acquisition of survey spectra and 20 eV for narrow scans. The base pressure in the sample chamber during analysis was approximately 3×10^{-8} mbar. Spectral analysis was carried out using the standard VGS 5000S software. Surface compositions (in atom%) were determined by considering the integrated peak areas of the C 1s, N 1s, S 2p and O 1s signals and their experimental sensitivity factors (0.25, 0.42, 0.54 and 0.66, respectively).

All measurements on copolymer–silica nanocomposites were

Table 1 Summary of bulk and surface compositional data obtained for four poly(4-vinylpyridine)–silica colloidal nanocomposites synthesized at varying initial concentrations of 4-vinylpyridine and silica sol. Reaction conditions: polymerizations were carried out at 60 °C for 24 h using 1.0% ammonium persulfate initiator, based on 4VP.

Monomer conc. (v/v%)	Initial silica conc. (w/v%)	Silica content (wt.%)	Silicon content[a] (wt.%)	Microanalysis (wt.%) N	XPS analysis (at.%) Si	XPS analysis (at.%) N	Bulk Si/N (at. ratio)	Surface Si/N (at. ratio)	$Si/N_{(surface)}$ to $Si/N_{(bulk)}$ ratio
5	8	36	17	7.8	8.2	8.6	1.07 ± 0.03	1.0 ± 0.1	0.9 ± 0.1
10	8	32	15	8.5	6.2	8.6	0.89 ± 0.03	0.7 ± 0.1	0.8 ± 0.1
5	16	37	17	7.9	7.0	8.6	1.09 ± 0.04	0.8 ± 0.1	0.7 ± 0.1
10	16	38	18	7.7	6.4	7.8	1.16 ± 0.04	0.8 ± 0.1	0.7 ± 0.1

[a]Wt.% Si calculated from TGA analysis assuming that residue is SiO_2.

made using a VG Scientific Sigma Probe spectrometer. This source was fitted with a monochromated Al-Kα source as standard and the equipment used in the current work was also fitted with a standard twin anode X-ray source providing Al-Kα or Mg-Kα photons. The spectra reported in this paper were all acquired using Mg-Kα ($h\upsilon = 1253.6$ eV) radiation and the analysis area was approximately 500 μm in diameter. The spectrometer was operated in the fixed analyser transmission mode and pass energies of 20 and 100 eV were used for the high resolution spectra and the survey spectra, respectively. For each sample, a survey spectrum was recorded together with core level spectra of the elements of interest (C 1s, N 1s, O 1s, Si 2p). Quantitative surface elemental compositions were determined using the peak areas of these spectra together with the appropriate sensitivity factors, using the software provided on the VG Scientific Eclipse data system. Peak fitting of the C1s spectra was carried with Eclipse software using a Gaussian peak shape with a 30% Lorentzian contribution.

Given that all the XPS samples were organic-based materials, the FWHM of the various components of a given spectrum were kept to within ±0.1 eV, except for the C 1s shake-up satellite peak centred at ~291 eV. The quality of the curve fit was obtained by the determination of χ^2, the sum of the squares of the difference between the experimental spectrum and the fitted envelope at 0.1 eV intervals over the peak region of interest. In performing the curve fitting, the best fits were always achieved within the constraints of chemical intuition. Charge referencing was achieved by setting the C ls component due to the CC/CH bonds at 285.0 eV and setting the main Si $2p_{3/2}$ component to 164.0 eV.

Identification of the N 1s peak from the poly(4-vinylpyridine) component of the nanocomposites was achieved by examining the XPS spectrum of the poly(4-vinylpyridine) reference material (Aldrich). Identification of the Si 2s peak was verified by XPS analysis of the 20 nm silica sol used to prepare the vinyl polymer–silica nanocomposites. The elemental ratios were estimated with an uncertainty of ±10% by adjusting the integrated peak areas using known sensitivity factors.[35] The chemical composition data presented in Tables 1 and 2 were used to determine the corresponding bulk Si/N atomic ratios for the copolymer nanocomposites. These calculated bulk Si/N atomic ratios are compared with the surface Si/N ratios measured by XPS in Tables 1 and 2.

Notation

In order to concisely describe the nanocomposites in this paper, a shorthand notation is used. Thus, '4VP/SiO_2' denotes a homopoly(4-vinylpyridine)–silica nanocomposite. Similarly, '78 : 22 St-4VP/SiO_2' denotes the *molar* composition of a styrene–4-vinylpyridine copolymer–silica nanocomposite, as calculated from nitrogen microanalyses.

Results and discussion

One of the chief advantages of XPS is its excellent inter-element resolution. On the other hand, intra-element resolution is poor and usually peak deconvolution or curve-fitting techniques are required to obtain useful information. In view of this limitation, we have always preferred, whenever possible, to exploit the presence of unique elemental markers when using XPS to characterize the surface compositions of multi-component colloidal particles.[23,36–38] In the present study, we have used the nitrogen signal arising from the 4VP auxiliary as a unique elemental marker for the (co)polymer component and silicon as a marker for the silica sol. In principle, carbon could be used as a marker for the (co)polymer, but in practice reliable quantification of this signal is often problematic due to variable surface contamination from adsorbed hydrocarbons, *etc.* (but see later).

Fig. 3 depicts the survey spectra recorded for the silica sol, a 4VP homopolymer, a 4VP/SiO_2 nanocomposite and a 78 : 22 St-4VP/SiO_2 nanocomposite. The silica sol contains signals due to silicon and oxygen, as expected. There is no detectable nitrogen signal at 398–402 eV. However, there is a weak signal due to carbon, which indicates either surface contamination or an intrinsic impurity in the silica sol. This unexpected observation again serves to illustrate the problem of using carbon as an elemental marker in XPS studies. The 4VP homopolymer contains strong signals due to nitrogen and carbon respectively. There is no detectable silicon signal between 100 and 170 eV. Thus, silicon and nitrogen serve as unique elemental markers for the silica and polymeric components of the nanocomposites, as anticipated. In the case of the 4VP/SiO_2 nanocomposite, signals due to both silicon (Si 2p) and nitrogen (N 1s) are observed. This means that both the inorganic and organic components are present at,

Table 2 Summary of bulk and surface compositional data for two copolymer–silica nanocomposites prepared by copolymerizing either styrene or methyl methacrylate with 4VP. Reaction conditions: 5.0 mL total monomer volume, 8.0 g (dry wt.%) silica sol, 100 mL total solvent volume, all polymerizations were carried out at 60 °C for 24 h

Entry no.	Comonomer type	4VP in final copolymer[a] (mol%)	Silica content (wt.%)	Silicon content[b] (wt.%)	Bulk analysis[c] (wt.%) C	Bulk analysis[c] (wt.%) N	XPS analysis (at.%) Si	XPS analysis (at.%) C	XPS analysis (at.%) N	Bulk Si/N (at. ratio)	Surface Si/N (at. ratio)	$Si/N_{(surface)}$ to $Si/N_{(bulk)}$ ratio
1	Styrene	22	25	11.2	66.8	2.17	13.3	48.3	2.5	2.7 ± 0.3	5.4 ± 0.8	2.00 ± 0.3
2	MMA	32	65	30.3	22.0	1.5	19.7	25.4	1.3	10 ± 1	15 ± 2	1.5 ± 0.3

[a]Determined from nitrogen microanalysis. [b]Wt.% Si calculated from TGA analysis assuming that residue is SiO_2. [c]As determined by microanalysis.

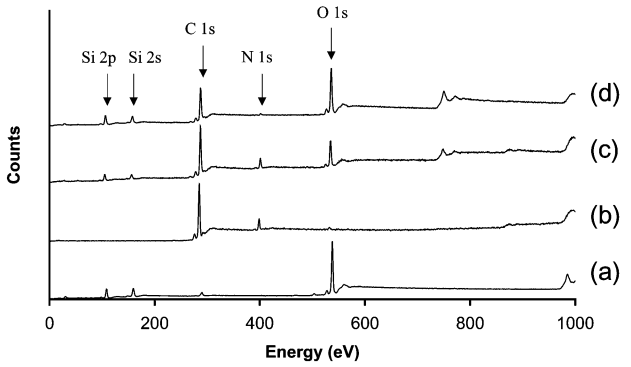

Fig. 3 XPS survey spectra of: (a) pristine silica sol; (b) poly(4-vinylpyridine) homopolymer; (c) 4VP/SiO_2 homopolymer nanocomposite; (d) 78 : 22 St-4VP/SiO_2 copolymer nanocomposite.

or very near (*i.e.* within the XPS sampling depth), the surface of the nanocomposite particles.

For quantification purposes, core line spectra were recorded for the elements of interest in each sample. Typical spectra are shown in Fig. 4. High quality, high signal-to-noise Si 2p and N 1s spectra were obtained for the 4VP/SiO_2 nanocomposite. Using known sensitivity factors, the surface concentrations of these elements can be determined. It is convenient to express this surface composition as an Si/N atomic ratio; these XPS data are summarized in Table 1 for four 4VP-SiO_2 nanocomposites prepared under various synthesis conditions. We have previously noted that the mean particle size and silica content of the 4VP/SiO_2 nanocomposites are relatively insensitive to the synthesis conditions.[26] It is clear from Table 1 that the surface compositions are also very similar. In each case, the Si/N ratios lie close to unity (0.7–0.9) and are comparable to the Si/N atomic ratios calculated from the bulk composition data (here the N% is determined directly by elemental microanalyses and the Si% is calculated indirectly from the incombustible TGA residues, which are assumed to be SiO_2). Thus the surface compositions of these 4VP/SiO_2 nanocomposites are very similar to their bulk compositions: if anything, the particle surface is slightly polymer-rich. These XPS observations are in striking contrast to our previous studies on a series of polypyrrole–silica (PPy/SiO_2) nanocomposites,[36] which invariably had markedly silica-rich surface compositions. This observation was interpreted as being consistent with the observed long-term colloid stability of these conducting polymer–silica particles. The vinyl polymer–silica nanocomposites in the present study also exhibit good long-term colloid stability. Presumably the surface concentration of silica, though not as high as for the conducting polymer–silica nanocomposites, is nevertheless sufficient to minimize particle aggregation. It is also possible that there is some contribution to the overall colloid stability from the polymeric component, since the ammonium persulfate initiator used in these nanocomposite syntheses is expected to lead to terminal anionic sulfate groups on most, if not all, of the polymer chains.[39]

With the copolymer–silica nanocomposites, most of the 4VP residues are replaced with either styrene or MMA residues, neither of which contains a nitrogen marker. Thus, in Fig. 3, the intensity of the N 1s signal due to the 4VP residues in a 78 : 22 St-4VP/SiO_2 nanocomposite is markedly weaker than that observed for the 4VP/SiO_2 nanocomposite. This is more clearly illustrated in Fig. 4(c), where the signal-to-noise ratio for the N 1s signal is significantly lower for the copolymer nanocomposite. This makes XPS analysis, and indeed nitrogen microanalysis, less accurate. Nevertheless, Si/N atomic ratios can be determined, although these data are obviously less reliable (see Table 2). In the case of the 78 : 22 St-4VP/SiO_2 nanocomposite, the Si/N surface atomic ratio of 5.4 $\pm$ 0.8 obtained from XPS is significantly greater than the bulk atomic ratio of 2.7 $\pm$ 0.3 determined from the combination of microanalytical and thermogravimetric data. This indicates that the surface of this nanocomposite is distinctly silica-rich. For the 68 : 32 MMA-4VP/SiO_2 nanocomposite, the Si/N surface atomic ratio is 15 $\pm$ 2 and the bulk atomic ratio is 10 $\pm$ 1, which is also consistent with a silica-rich particle surface.

The XPS differences between the two types of nanocomposites are also supported by aqueous electrophoresis measurements. Fig. 5 illustrates the zeta potential *vs.* pH curves obtained for the original 20 nm silica sol, a 4VP/SiO_2 homopolymer nanocomposite, a 78 : 22 St-4VP copolymer nanocomposite and a PPy/SiO_2 nanocomposite. In an earlier paper from our group, it was reported that the electrophoretic data for a series of conducting polymer–silica nanocomposites were superimposable on those obtained for a silica sol.[40]

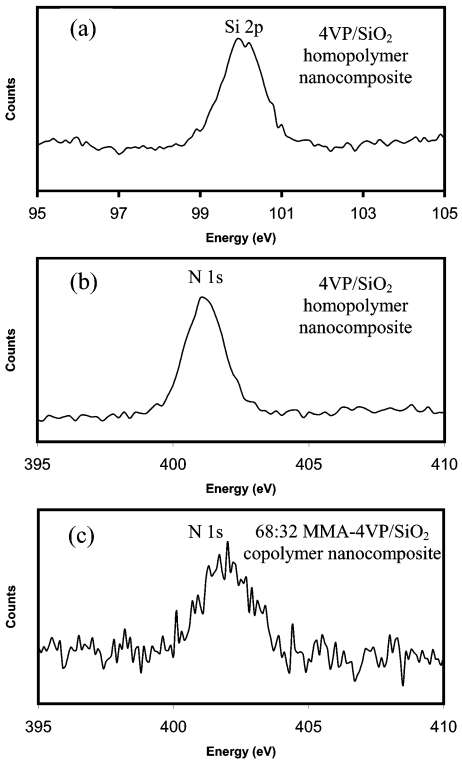

Fig. 4 Typical XPS silicon and nitrogen core line spectra obtained for vinyl (co)polymer–silica nanocomposites. (a) Si 2p core line spectrum for a 4VP/SiO_2 homopolymer nanocomposite; (b) N 1s core line spectrum for a 4VP/SiO_2 homopolymer nanocomposite; (c) N 1s core line spectrum for a 68 : 32 MMA-4VP/SiO_2 copolymer nanocomposite.

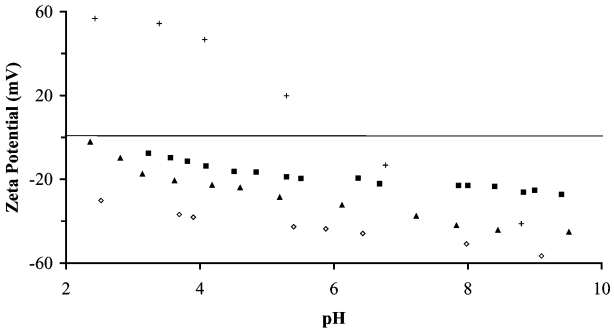

Fig. 5 Aqueous electrophoresis data for three polymer–silica nanocomposites and the ultrafine silica sol employed in their syntheses. (◊) 20 nm Nyacol 2040 silica sol, (+) 4VP-SiO_2 nanocomposite, (▲) PPy-SiO_2 nanocomposite (■) 78 : 22 St-4VP/SiO_2 nanocomposite.

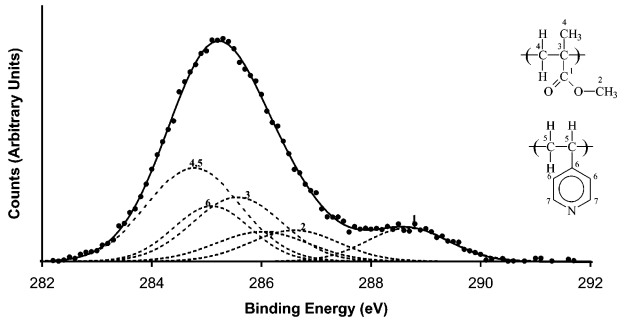

Fig. 6 Deconvoluted C 1s core line XPS spectrum of 68 : 32 MMA-4VP/SiO_2 copolymer nanocomposite. (●) Observed data; (—) theoretical calculated spectrum; (- - -) individual C 1s components.

However, the silica sol in question was not the same silica sol used to prepare the conducting polymer–silica nanocomposites.[41] Using a more modern instrument, the zeta potential *vs.* pH curve for the ultrafine Nyacol silica sol can now be determined directly. This curve is significantly more negative than that of the PPy/SiO_2 nanocomposite over the whole pH range studied (see Fig. 5). Nevertheless, the general shapes of these two curves are similar, which is consistent with a silica-rich surface composition for the PPy/SiO_2 nanocomposite particles, as previously indicated by XPS measurements.[36] Similarly, the 78 : 22 St-4VP/SiO_2 copolymer nanocomposite exhibits negative zeta potentials at all pH, which also suggests that these particles have a silica-rich surface composition. This is borne out by our XPS observations in the present study (see above). In contrast, a classical 'S' shaped curve is obtained with the 4VP-SiO_2 nanocomposite. A well-defined isoelectric point is observed at around pH 6; below this pH, positive zeta potentials are observed, presumably due to protonation of the basic 4VP residues at the particle surface. This interpretation is again consistent with the XPS results discussed above, which indicate the presence of the 4VP homopolymer at the surface of the nanocomposite particles.

Although the N 1s signal is a perfectly good marker for the polymeric component in 4VP/SiO_2 homopolymer nanocomposites, it can be less useful for copolymer–silica nanocomposites, since the 4VP comonomer is usually present at a reduced concentration (up to an order of magnitude lower). In view of this limitation, we explored the possibility of using the carbonyl carbon signal as an elemental marker for MMA-4VP/SiO_2 nanocomposites. As stated earlier, quantification of the C 1s signal is generally rather unreliable due to surface contamination effects, but this problem does not apply to the carbonyl carbon component, which is due solely to the MMA residues in the copolymer. Moreover, unlike most sub-peaks, the carbonyl carbon is partially resolved from the main C 1s peak, which makes curve fitting much less problematic and reduces the possibility of error. Fig. 6 depicts a typical curve-fitted C 1s envelope obtained for the 68 : 32 MMA-4VP/SiO_2 nanocomposite in Table 2. The carbonyl carbon signal is clearly discernible at around 289 eV and curve fitting based on likely peak widths and chemical intuition allows reliable quantification. Thus, the percentage contribution that the carbonyl carbon component makes to the total C 1s peak is determined. This enables calculation of the Si/C=O surface atomic ratio, which is 7 $\pm$ 1. The corresponding Si/C=O bulk atomic ratio of 4.9 $\pm$ 0.8 is readily calculated from the microanalytical carbon content of the nanocomposite (see Table 2), allowing for the 4VP content of the copolymer (determined by N microanalysis) and the fact that only one in five carbons in the MMA residues is a carbonyl carbon. The ratio of Si/C=O(surface) to Si/C=O(bulk) is 1.5 $\pm$ 0.4, which is in very good agreement with the Si/N(surface) to Si/N(bulk) ratio of 1.5 $\pm$ 0.3 (see final column in Table 2). Clearly, there is reasonable agreement between the nitrogen signal and the carbonyl carbon signal analyses in this particular case. We have also observed similarly good agreement with related nanocomposite particles in unpublished studies. However, it is worth emphasizing that the carbonyl carbon approach is likely to be more reliable for MMA-based nanocomposites containing much lower (or zero) amounts of 4VP comonomer. Obviously, this carbonyl carbon marker method works best for MMA (and perhaps also methyl acrylate); it is not applicable to styrene and it is inherently less accurate for methacrylic comonomers such as *n*-butyl methacrylate, since in this case only one in eight carbon atoms per repeat unit is a carbonyl carbon.

Finally, cryo-ultramicrotomy techniques were used to prepare sectioned 4VP/SiO_2 and 78 : 22 St : 4VP/SiO_2 nanocomposite particles for TEM examination, see Fig. 7. For the 4VP/SiO_2 nanocomposite, there is clear evidence for the distribution of the silica sol throughout the particle interior. This is consistent with the XPS data and the 'currant bun'

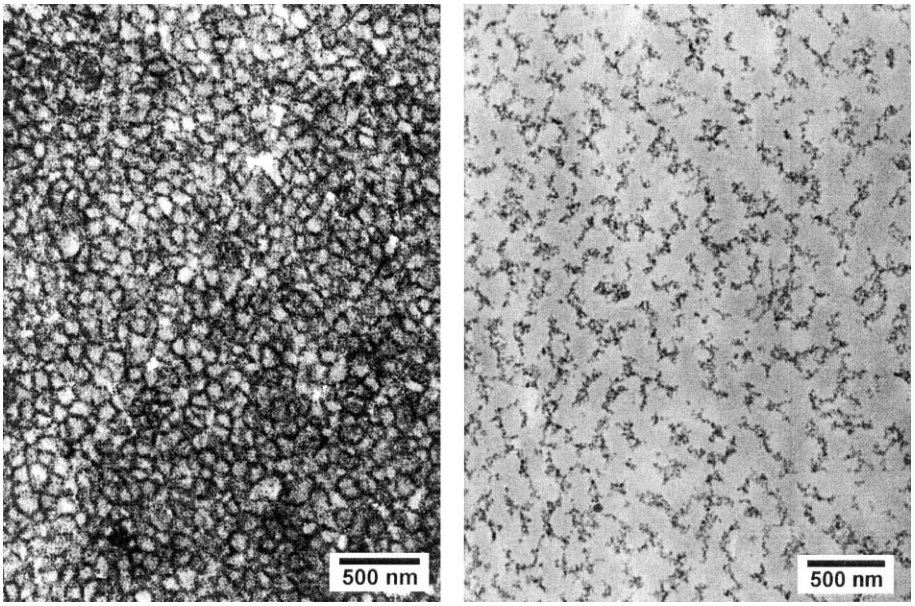

Fig. 7 Cryo-TEM images of ultra-thin sections of: (a) the 4VP/SiO_2 homopolymer nanocomposite and (b) the 78 : 22 St-4VP/SiO_2 copolymer nanocomposite.

particle morphology proposed in our earlier papers. In contrast, the 78 : 22 St : 4VP/SiO_2 nanocomposite appears to have a distinctive core–shell morphology, with the silica sol solely located on the outside of the particles.[42] This is understandable, since polystyrene is relatively hydrophobic compared to poly(4-vinylpyridine) and thus surface thermodynamics should tend to exclude the polystyrene more strongly from the air–water interface in favor of the highly hydrophilic silica sol. Unfortunately, cryo-ultramicrotomy was not carried out on the 68 : 32 MMA-4VP/SiO_2 nanocomposite. However, in view of their relatively high silica content (65% by mass), a 'raspberry' morphology is suggested for these particles.

Conclusions

Using the unique elemental marker approach, surface silicon/nitrogen atomic ratios were determined by XPS in order to assess the surface compositions of selected nanocomposite particles. All the homopoly(4-vinylpyridine)–silica nanocomposites examined had surface compositions that were comparable to their bulk compositions, which indicates that the silica particles are uniformly distributed throughout these nanocomposites. In contrast, a poly(styrene-co-4-vinylpyridine)–silica nanocomposite was distinctly silica-rich as judged by XPS, which suggests a core–shell morphology. Both of these proposed particle morphologies were supported by cryo-ultramicrotomy TEM studies. A poly(methyl methacrylate-co-4-vinylpyridine)–silica nanocomposite had an XPS surface composition which was intermediate between those found for the 'currant bun' particles and the core–shell particles. In view of its relatively high silica content, a 'raspberry' particle morphology was suggested. In the case of the poly(methyl methacrylate-co-4-vinylpyridine)–silica nanocomposite, it was demonstrated that the carbonyl carbon signal of the methyl methacrylate residues can also act as an unambiguous marker for the copolymer component; the surface composition obtained from this alternative analysis was consistent with that calculated using the nitrogen XPS signal. This carbonyl carbon approach may be particularly useful for assessing the surface compositions of nanocomposites prepared in the presence of little or no 4-vinylpyridine comonomer.

Acknowledgement

The EPSRC is acknowledged for a post-doctoral research grant (GR/M22017) for M. J. P. We thank Dr Heckmann and Mr Heiter (BASF, Germany) for their kind assistance in obtaining the TEM images. Eka Chemicals (Bohus, Sweden) is thanked for the donation of the 20 nm silica sol. The Comisión de Investigaciones Científicas de la Provincia de Buenos Aires (CICPBA) is thanked for allowing J. I. A. a one-year secondment at the University of Sussex.

References

1 A. Usuki, Y. Kojima, M. Kawasumi, A. Okada, Y. Fukushima, T. Kurauchi and O. Kamigaito, *J. Mater. Res.*, 1993, **8**, 1179.
2 Y. Kojima, A. Asuuki, M. Kuwasumi, A. Okada, Y. Fukushima, T. Kurauchi and O. Kamigaito, *J. Mater. Res.*, 1993, **8**, 1185.
3 A. Okada and A. Usuki, *Mater. Sci. Eng.*, 1995, **C3**, 109.
4 J. W. Gilman, C. L. Jackson, A. B. Morgan, R. Harris, E. Manias, E. P. Giannelis, M. Wuthenow, D. Hilton and S. H. Phillips, *Chem. Mater.*, 2000, **12**, 1866.
5 C. P. Mehnet and J. Ying, *Chem. Commun.*, 1997, 2215.
6 J. K. Vassilon, R. P. Ziebarth and F. J. Disalvo, *Chem. Mater.*, 1990, **2**, 738.
7 T.-W. Lee, O. O. Park, J. Yoon and J.-J. Kim, *Adv. Mater.*, 2001, **13**, 211.
8 M. Biswas and S. S. Ray, *Adv. Polym. Sci.*, 2001, **155**, 167.
9 (*a*) Z. C. Pu, J. E. Mark, J. M. Jethmalani and W. T. Ford, *Chem. Mater.*, 1997, **9**, 2442; (*b*) Z. C. Pu, J. E. Mark, J. M. Jethmalani and W. T. Ford, *Polym. Bull.*, 1996, **37**, 545.
10 J. W. Gilman, C. L. Jackson, A. B. Morgan, R. Harris Jr., E. Manias, E. P. Giannelis, M. Wuthenow, D. Hilton and S. H. Phillips, *Chem. Mater.*, 2000, **12**, 1866.
11 A. B. Morgan, J. M. Atomucci, M. R. van Landingham, R. H. Harris and T. Kashiwagi, *Abstr. Pap. Am. Chem. Soc.*, 2000, **220**, 67-PMSE part 2.
12 R. KIler and H. J. McQueston, *US Pat.* 4 010 242, 1977.
13 E. Bourgeat-Lami and J. Lang, *J. Colloid Interface Sci.*, 1998, **197**, 293.
14 E. Bourgeat-Lami and J. Lang, *J. Colloid Interface Sci.*, 1999, **210**, 281.
15 M. Gill, J. Mykytiuk, S. P. Armes, J. L. Edwards, T. Yeates, P. J. Moreland and C. Mollett, *J. Chem. Soc., Chem. Commun.*, 1992, 108.
16 S. Maeda and S. P. Armes, *J. Colloid Interface Sci.*, 1993, **159**, 257.
17 S. Maeda and S. P. Armes, *J. Mater. Chem.*, 1994, **4**, 935.
18 S. Maeda and S. P. Armes, *Chem. Mater.*, 1995, **7**, 171.
19 S. Maeda and S. P. Armes, *Synth. Met.*, 1995, **73**, 151.
20 R. Flitton, J. Johal, S. Maeda and S. P. Armes, *J. Colloid Interface Sci.*, 1995, **173**, 135.
21 G. P. McCarthy, S. P. Armes, S. J. Greaves and J. F. Watts, *Langmuir*, 1997, **13**, 3686.
22 M. I. Goller, C. Barthet, G. P. McCarthy, R. Corradi, B. P. Newby, S. A. Wilson, S. P. Armes and S. Y. Luk, *Colloid Polym. Sci.*, 1998, **276**, 1010.
23 S. Maeda, R. Corradi and S. P. Armes, *Macromolecules*, 1995, **28**, 2905.
24 M. R. Pope, S. P. Armes and P. J. Tarcha, *Bioconjugate Chem.*, 1996, **7**, 436.
25 C. Barthet, A. J. Hickey, D. B. Cairns and S. P. Armes, *Adv. Mater.*, 1999, **11**, 408.
26 M. J. Percy, C. Barthet, J. C. Lobb, M. A. Khan, M. Vamvakaki, S. F. Lascelles and S. P. Armes, *Langmuir*, 2000, **16**, 6913.
27 J. I. Amalvy, M. J. Percy, S. P. Armes and H. Wiese, *Langmuir*, 2001, **17**, 4770.
28 D. Briggs and M. P. Seah, *Practical Surface Analysis*, Wiley, Chichester, 2nd edn., 1990, vol. 1.
29 M. C. Davies, R. A. P. Lynn, J. Hearn, A. J. Paul, J. C. Vickerman and J. F. Watts, *Langmuir*, 1996, **12**, 3866.
30 Y. Deslandes, D. F. Mitchell and A. Paine, *Langmuir*, 1993, **9**, 1468.
31 M. C. Davies, R. A. P. Lynn, S. S. Davis, J. Hearn, J. F. Watts, J. C. Vickerman and A. J. Paul, *Langmuir*, 1993, **9**, 1637.
32 M. C. Davies, R. A. P. Lynn, S. S. Davis, J. Hearn, J. F. Watts, J. C. Vickerman and D. Johnson, *Langmuir*, 1994, **10**, 1399.
33 M. C. Davies, R. A. P. Lynn, J. Hearn, A. J. Paul, J. C. Vickerman and J. F. Watts, *Langmuir*, 1995, **11**, 4313.
34 R. J. Hunter, *Foundations of Colloid Science*, Clarendon Press, Oxford, 1989, vol. 2.
35 J. F. Moulder, W. F. Stickle, P. E. Sobol and K. D. Bomben, *Handbook of X-ray Photoelectron Spectroscopy*, ed. J. Chastain, Perkin-Elmer Corporation, Minnesota, USA, 1992.
36 S. Maeda, M. Gill, S. P. Armes and I. W. Fletcher, *Langmuir*, 1995, **11**, 1899.
37 D. B. Cairns, S. P. Armes, M. M. Chehimi, C. Perruchot and M. Delamar, *Langmuir*, 1999, **15**, 8059.
38 M. A. Khan, S. P. Armes, C. Perruchot, H. Ouamara, M. M. Chehimi, S. J. Greaves and J. F. Watts, *Langmuir*, 2000, **16**, 4171.
39 M. Okubo, Y. Konishi and H. Minami, *Colloid Polym. Sci.*, 2001, **279**, 519.
40 M. D. Butterworth, S. Maeda, J. Johal, R. Corradi, S. F Lascelles and S. P Armes, *J. Colloid Interface Sci.*, 1995, **174**, 510.
41 This was due to the limited particle size range of the PenKem instrument used in ref. 40, which could not detect the ultrafine 20 nm Nyacol silica sol. Thus, a much larger 500 nm Deltech silica sol was used for the electrophoresis measurements and it was assumed that the surface chemistry of the Nyacol silica sol was identical to that of the Deltech sol. In retrospect, this assumption was not valid.
42 Note that a 'raspberry' morphology was tentatively proposed in our earlier paper.